

Article

Nonequilibrium Casimir-Polder Force between Nanoparticles and Graphene-Coated Silica Plate: Combined Effect of the Chemical Potential and Mass Gap

Galina L. Klimchitskaya ^{1,2,*} , Constantine C. Korikov³ and Vladimir M. Mostepanenko ^{1,2,4} 

¹ Central Astronomical Observatory at Pulkovo of the Russian Academy of Sciences, 196140 Saint Petersburg, Russia

² Peter the Great Saint Petersburg Polytechnic University, 195251 Saint Petersburg, Russia

³ Huawei Noah's Ark Lab, Krylatskaya str. 17, Moscow 121614, Russia

⁴ Kazan Federal University, 420008 Kazan, Russia

* Correspondence: g.klimchitskaya@gmail.com

Abstract: The Casimir-Polder force between spherical nanoparticles and a graphene-coated silica plate is investigated in situations out of thermal equilibrium, i.e., with broken time-reversal symmetry. The response of graphene coating to the electromagnetic field is described on the basis of first principles of quantum electrodynamics at nonzero temperature using the formalism of the polarization tensor in the framework of the Dirac model. The nonequilibrium Casimir-Polder force is calculated as a function of the mass-gap parameter, chemical potential of graphene and temperature of the graphene-coated plate, which can be both higher and lower than that of the environment. It is shown that the force value increases with increasing chemical potential, and this increase is more pronounced when the temperature of a graphene-coated plate is lower than that of the environment. The nonequilibrium force also increases with increasing temperature of the graphene-coated plate. This increase is larger when the plate is hotter than the environment. The effect is revealed that the combined impact of the chemical potential μ and mass gap Δ of graphene coating depends on the relationship between Δ and 2μ . If $2\mu > \Delta$ the magnitude of the nonequilibrium force between nanoparticles and a cooled graphene-coated plate becomes much larger than for a graphene coating with $\mu = 0$. The physical reasons explaining this effect are elucidated. Possible applications of the obtained results are discussed.

Keywords: Casimir-Polder interaction out of thermal equilibrium; graphene-coated plates; mass gap; chemical potential; polarization tensor along the real frequency axis; nanoparticles

1. Introduction

The two-dimensional (2D) hexagonal lattice of carbon atoms called graphene [1] has attracted particular attention of many experts in both fundamental and applied physics because at low energies it adequately fits the requirements of the Dirac model. What this means is that graphene can be considered as consisting of light quasiparticles described not by the Schrödinger equation, as is customary in condensed matter physics, but by the relativistic Dirac equation in 2D space and one-dimensional (1D) time, where the speed of light c is replaced with the Fermi velocity $v_F \approx c/300$ [2].

For experts in fundamental physics, graphene is interesting because it possesses unusual electrical, optical and mechanical properties which offer outstanding possibilities to large-scale exploratory investigations [3,4]. At the same time, graphene suggests a wide range of prospective applications in nanotechnology and material science [5,6]. Specifically, certain of the nanotechnological devices rely upon interaction between nanoparticles and graphene-coated plates for their operation [7–12].

arXiv:2403.05983v1 [quant-ph] 9 Mar 2024



Citation: Klimchitskaya, G.L.; Korikov, C.C.; Mostepanenko, V.M. Nonequilibrium Casimir-Polder Force between nanoparticles and Graphene-Coated Silica Plate: Combined Effect of the Chemical Potential and Mass Gap. *Symmetry* **2024**, *16*, 320. <https://doi.org/10.3390/sym16030320>

Received: 12 January 2024

Revised: 16 February 2024

Accepted: 1 March 2024

Published: 7 March 2024



Copyright: © 2024 by the authors. Licensee MDPI, Basel, Switzerland. This article is an open access article distributed under the terms and conditions of the Creative Commons Attribution (CC BY) license (<https://creativecommons.org/licenses/by/4.0/>).

The Casimir-Polder force [13] acting between an electrically neutral microscopic particle and a material plate is the relativistic and quantum phenomenon. It is initiated by the zero-point and thermal fluctuations of the electromagnetic field. In the state of thermal equilibrium, when temperatures of the microparticle, plate, and of the environment are equal, the Casimir-Polder force is described by the Lifshitz theory [14–16]. This theory expresses the force value via the dynamic polarizability of a particle and the frequency-dependent dielectric permittivity of the plate material.

There is an extensive literature devoted to calculations of the Casimir-Polder force between atoms, molecules, nanoparticles and diversified material surfaces, including graphene, by means of the Lifshitz theory (see, e.g., Refs. [17–44]). In doing so, the spatially nonlocal dielectric permittivities and the 2D reflection coefficients of graphene sheets [45] were expressed via the polarization tensor of graphene in (2+1) dimensional space-time [46–49] in the framework of the Dirac model.

In some instances, the condition of thermal equilibrium is violated with the result that the Lifshitz theory becomes inapplicable. For example, this may happen in the applications of graphene to solar cells where the graphene-coated plate has different temperature from that of nanoparticles and of the environment [50,51]. Although almost all physical theories, including the Lifshitz theory, are symmetric relatively to the operation of time reversal, in thermally nonequilibrium systems this symmetry is broken.

The generalization of the Lifshitz theory to the cases when the condition of thermal equilibrium is violated was developed under an assumption that each body in the physical system under consideration is in the state of local thermal equilibrium [52–55]. As a result, it has become possible to calculate the Casimir-Polder force in situations when the temperature of a plate, a nanoparticle, an even of the environment are dissimilar.

The theory of nonequilibrium Casimir and Casimir-Polder forces was further generalized to the case of nonplanar configurations [56–60] and for the plate materials with temperature-dependent dielectric permittivities [61–65]. It was also confirmed experimentally by measuring the nonequilibrium Casimir-Polder force between the Bose-Einstein condensate of ^{87}Rb atoms and a SiO_2 plate, which was heated as compared to the environmental temperature [66].

Investigation of the nonequilibrium Casimir-Polder interaction between spherical nanoparticles and graphene sheet using the formalism of the polarization tensor has been started by Ref. [67]. In that work, the pristine graphene sheet freestanding in vacuum was considered. This means that the crystal lattice of graphene was assumed to be perfect with no foreign atoms and gapless quasiparticle spectrum. According to the results of Ref. [67], the impact of nonequilibrium conditions on the total Casimir-Polder force is the most pronounced at short separations between a nanoparticle and a graphene sheet. At these separations, the force may even change its sign and become repulsive.

Real graphene sheets are, however, not pristine and, specifically, the quasiparticles in graphene, although light, are not massless. This leads to some nonzero mass gap Δ in the quasiparticle spectrum [3,68,69]. An impact of the nonzero mass gap on the nonequilibrium Casimir-Polder interaction between nanoparticles and a freestanding in vacuum graphene sheet was investigated in Ref. [70] within the formalism of the polarization tensor. It was shown that in this case the nonequilibrium Casimir-Polder force remains attractive and it is possible to control its value by varying the mass-gap parameter.

The freestanding graphene sheets are difficult, if not impossible, to use in physical experiments and in nanodevices, where they are usually deposited on some dielectric plates. An impact of the plate material on the nonequilibrium Casimir-Polder force between nanoparticles and a silica plate coated with gapped graphene was considered in Ref. [71]. It was shown that the presence of a silica plate increases the magnitude of the nonequilibrium Casimir-Polder force. With increasing mass-gap parameter, the magnitude of the nonequilibrium force decreases and the impact of graphene coating on the force becomes smaller.

It should be noted that computations of the nonequilibrium Casimir-Polder force acting on nanoparticles from real graphene sheet using the polarization tensor are rather cumbersome. They are connected with calculation of the multiple integrals of rapidly varying functions and were realized on a supercomputer [70,71].

In addition to the nonzero mass gap, real graphene sheets are unavoidably doped, i.e., contain some fraction of foreign atoms described by the nonzero value of the chemical potential μ [3,72,73]. This should be taken into account in the theoretical computations intended for the comparison with the measurement data as was successfully done in the experiment on measuring the equilibrium Casimir force acting between an Au-coated sphere and a graphene-coated SiO₂ plate [74,75].

The nonequilibrium Casimir interaction between two plates coated with the gapless graphene sheets possessing the nonzero chemical potential was investigated in Ref. [76] using the phenomenological, spatially local, model for the response of graphene to the electromagnetic field [72,77].

In this paper, we investigate the Casimir-Polder force acting between spherical nanoparticles and fused silica plate coated with gapped and doped graphene sheet in situations out of thermal equilibrium using the formalism of the polarization tensor. It is assumed that the temperature of nanoparticles is the same as of the environment. However, the temperature of the graphene-coated plate can be either lower or higher than that of the environment. The spatially nonlocal response of graphene to the fluctuating electromagnetic field is described by the polarization tensor, which takes into account the dependence of graphene properties on temperature, on the mass-gap parameter, and on the chemical potential. In doing so, the explicit expressions for the polarization tensor along the real frequency axis are presented in the region of evanescent waves. The obtained results for the nonequilibrium Casimir-Polder force are compared with those for the equilibrium one in the same configuration.

It is shown that increasing of the chemical potential of graphene coating leads to the monotonous increase of both the equilibrium and nonequilibrium Casimir-Polder forces between a nanoparticle and a graphene-coated plate. In doing so, for a heated graphene-coated plate, the mass gap makes a lesser impact on the force if the chemical potential takes a nonzero value. According to our results, for a cooled graphene-coated plate the impact of chemical potential of graphene coating on the nonequilibrium Casimir-Polder force essentially depends on whether the inequality $2\mu > \Delta$ or $2\mu < \Delta$ is satisfied. By and large, the impact of chemical potential on the nonequilibrium force for a cooled graphene-coated plate is stronger than for a heated one.

The paper is organized as follows. In Section 2, both the formalism of the Lifshitz theory and the computational results for the equilibrium Casimir-Polder force between nanoparticles and a silica plate coated with gapped and doped graphene sheet are presented. Section 3 contains the generalization of the Lifshitz theory of Casimir-Polder force for the out-of-thermal-equilibrium conditions and the required expressions for the polarization tensor of graphene along the real frequency axis with due regard for different relationships between the mass gap and chemical potential of graphene coating. In Section 4, the computational results for the nonequilibrium Casimir-Polder force as a function of separation are presented under different values of temperature, mass gap and chemical potential of graphene coating. In Section 5, the reader will find a discussion of the obtained results. Section 6 contains our conclusions.

2. Equilibrium Casimir-Polder Force between Nanoparticles and Silica Plate Coated with Gapped and Doped Graphene

We consider the spherical nanoparticles of radius R spaced above large, graphene-coated fused silica (SiO₂) plate at height $a \gg R$. The graphene coating is characterized by the mass gap Δ and chemical potential μ . The fused silica plate chosen for computations is the most typical substrate used as a supporter for graphene [74,75,78–81]. All below equations are, however, applicable to any material substrate.

The temperature of the environment is $T_E = 300$ K. In this section, the temperature of graphene-coated plate, T_p , is equal to T_E : $T_p = T_E = 300$ K. Nanoparticle temperature is assumed to be equal to T_E throughout the paper. We also assume that at all temperatures T considered below the nanoparticle radius satisfies the condition $R \ll \hbar c / (k_B T)$, where \hbar is the reduced Planck constant, c is the speed of light, and k_B is the Boltzmann constant. At $T = T_E$ this condition reduces to the inequality $R \ll 7.6 \mu\text{m}$. When it is satisfied, the dynamic polarizability of nanoparticle $\alpha(\omega)$ at all frequencies ω contributing to the Casimir-Polder force is approximately equal to the static value $\alpha(0)$ [59].

In the situation of thermal equilibrium $T_p = T_E$, the Casimir-Polder force between a nanoparticle and a graphene-coated plate is given by the Lifshitz formula written in terms of the discrete Matsubara frequencies [14–16,82,83]. Keeping in mind application of the same notations in the next section devoted to the situation out of thermal equilibrium, in this section we continue to denote the plate and environment temperatures as T_p and T_E but imply that $T_p = T_E = 300$ K. Then, the equilibrium Casimir-Polder force between a nanoparticle and a graphene-coated SiO₂ plate is given by [14–16,82,83]

$$F_{\text{eq}}^{\text{SiO}_2}(a, \Delta, \mu, T_E, T_p) = -\frac{2k_B T_E \alpha(0)}{c^2} \sum_{l=0}^{\infty} \int_0^{\infty} k dk e^{-2aq_{E,l}(k)} \times \left\{ \left[2q_{E,l}^2(k)c^2 - \zeta_{E,l}^2 \right] R_{\text{TM}}(i\zeta_{E,l}, k, \Delta, \mu, T_p) - \zeta_{E,l}^2 R_{\text{TE}}(i\zeta_{E,l}, k, \Delta, \mu, T_p) \right\}. \quad (1)$$

Here, k is the magnitude of the wave vector projection on the plane of graphene-coated plate, the Matsubara frequencies are $\zeta_{E,l} = 2\pi k_B T_E l / \hbar$ with $l = 0, 1, 2, \dots$, the prime on the summation sign means that the term with $l = 0$ is divided by 2, and

$$q_{E,l}(k) = \left(k^2 + \frac{\zeta_{E,l}^2}{c^2} \right)^{1/2}. \quad (2)$$

The reflection coefficients on the graphene-coated plate for the electromagnetic fluctuations with transverse magnetic (TM) and transverse electric (TE) polarizations are expressed via the dielectric permittivity of the plate material $\varepsilon(\omega)$ and the polarization tensor of graphene $\Pi_{\beta\gamma}(\omega, k, \Delta, \mu, T_p)$ calculated at the pure imaginary Matsubara frequencies [40,74,75,84]

$$R_{\text{TM}}(i\zeta_{E,l}, k, \Delta, \mu, T_p) = \frac{\hbar k^2 [\varepsilon(i\zeta_{E,l}) q_{E,l}(k) - q_{E,l}^\varepsilon(k)] + q_{E,l}(k) q_{E,l}^\varepsilon(k) \Pi_{00}(i\zeta_{E,l}, k, \Delta, \mu, T_p)}{\hbar k^2 [\varepsilon(i\zeta_{E,l}) q_{E,l}(k) + q_{E,l}^\varepsilon(k)] + q_{E,l}(k) q_{E,l}^\varepsilon(k) \Pi_{00}(i\zeta_{E,l}, k, \Delta, \mu, T_p)},$$

$$R_{\text{TE}}(i\zeta_{E,l}, k, \Delta, \mu, T_p) = \frac{\hbar k^2 [q_{E,l}(k) - q_{E,l}^\varepsilon(k)] - \Pi(i\zeta_{E,l}, k, \Delta, \mu, T_p)}{\hbar k^2 [q_{E,l}(k) + q_{E,l}^\varepsilon(k)] + \Pi(i\zeta_{E,l}, k, \Delta, \mu, T_p)}. \quad (3)$$

Here,

$$q_{E,l}^\varepsilon(k) = \left[k^2 + \varepsilon(i\zeta_{E,l}) \frac{\zeta_{E,l}^2}{c^2} \right]^{1/2} \quad (4)$$

and the following combination of the components of the polarization tensor is introduced:

$$\Pi(i\zeta_{E,l}, k, \Delta, \mu, T_p) \equiv k^2 \Pi_\beta^\beta(i\zeta_{E,l}, k, \Delta, \mu, T_p) - q_{E,l}^2(k) \Pi_{00}(i\zeta_{E,l}, k, \Delta, \mu, T_p), \quad (5)$$

where a summation over the repeated index $\beta = 0, 1, 2$ is implied.

For numerical computations of the equilibrium Casimir-Polder force (1) between a nanoparticle and a graphene-coated substrate, one needs the values of the static polarizability of a nanoparticle, $\alpha(0)$, of the dielectric permittivity of plate material, $\varepsilon(i\zeta_{E,l})$, and of the components of the polarization tensor of graphene, $\Pi_{00}(i\zeta_{E,l}, k, \Delta, \mu, T_p)$ and $\Pi(i\zeta_{E,l}, k, \Delta, \mu, T_p)$.

The static polarizability of spherical nanoparticles made of dielectric material is [59] $\alpha(0) = R^3[\varepsilon(0) - 1]/[\varepsilon(0) + 2]$. Thus, for nanoparticles made of high-resistivity Si one obtains $\varepsilon(0) = 3.81$ and $\alpha(0) = 0.484R^3$. For metallic nanoparticles, $\varepsilon(0) = \infty$ and $\alpha(0) = R^3$.

The dielectric permittivity of SiO₂ at the pure imaginary Matsubara frequencies is obtained from the optical data for the imaginary part of $\varepsilon(\omega)$ [85] with the help of the Kramers-Kronig relation. The obtained values were repeatedly used in calculations of the Casimir and Casimir-Polder forces [82]. There are also analytic expressions for the dielectric permittivity of SiO₂ along the imaginary frequency axis [86,87].

Below we present the components of the polarization tensor of gapped and doped graphene at the Matsubara frequencies found in the framework of the Dirac model [46–49]. As mentioned in Section 1, this model is applicable at low energies. In Ref. [88] the upper boundary of its application region is estimated as 3 eV. Thus, one should consider not too small separations a between the nanoparticle and the graphene-coated plate in order that all energies giving the major contribution to the Casimir-Polder interaction lie below this boundary.

It has been known that the characteristic energy of the Casimir-Polder interaction is equal to $\hbar c/(2a)$ [82,89]. This energy is less than 1 eV at all separation distances $a > 100$ nm. That is why, at separations exceeding, e.g., 200 nm one can reliably use the polarization tensor of graphene derived in the framework of the Dirac model. This conclusion was confirmed by measurements of the Casimir force between an Au-coated sphere and a graphene-coated SiO₂ plate, which were found in a very good agreement with theoretical predictions using the polarization tensor of graphene [74,75].

The explicit expression for the component Π_{00} of the polarization tensor is given by [40,74,75]

$$\begin{aligned} \Pi_{00}(i\zeta_{E,l}, k, \Delta, \mu, T_p) &= \frac{\alpha\hbar k^2}{\tilde{q}_{E,l}(k)} \Psi(D_{E,l}) + \frac{4\alpha\hbar c^2 \tilde{q}_{E,l}(k)}{v_F^2} \int_{D_{E,l}}^{\infty} du w_{E,l}(u, k, \mu, T_p) \\ &\times \left[1 - \operatorname{Re} \frac{1 - u^2 + 2i\gamma_{E,l}u}{(1 - u^2 + 2i\gamma_{E,l}u + D_{E,l}^2 - \gamma_{E,l}^2 D_{E,l}^2)^{1/2}} \right], \end{aligned} \quad (6)$$

where $\alpha = e^2/(\hbar c)$ is the fine structure constant and the following notations are introduced

$$\begin{aligned} \Psi(x) &= 2 \left[x + (1 - x^2) \arctan \frac{1}{x} \right], \quad D_{E,l} = \frac{\Delta}{\hbar c \tilde{q}_{E,l}(k)}, \\ \tilde{q}_{E,l}(k) &= \frac{1}{c} \sqrt{v_F^2 k^2 + \zeta_{E,l}^2}, \quad \gamma_{E,l} = \frac{\zeta_{E,l}}{c \tilde{q}_{E,l}(k)}, \\ w_{E,l}(u, k, \mu, T_p) &= \sum_{\kappa=\pm 1} \left(e^{B_{E,l}u + \kappa \frac{\mu}{k_B T_p}} + 1 \right)^{-1}, \quad B_{E,l} = \frac{\hbar c \tilde{q}_{E,l}(k)}{2k_B T_p}. \end{aligned} \quad (7)$$

In a similar way, the explicit expression for the combination of the components of the polarization tensor Π takes the form [40,74,75]

$$\begin{aligned} \Pi(i\zeta_{E,l}, k, \Delta, \mu, T_p) &= \alpha\hbar k^2 \tilde{q}_{E,l}(k) \Psi(D_{E,l}) - \frac{4\alpha\hbar \tilde{q}_{E,l}(k) \zeta_{E,l}^2}{v_F^2} \int_{D_{E,l}}^{\infty} du w_{E,l}(u, k, \mu, T_p) \\ &\times \left[1 - \operatorname{Re} \frac{(1 + i\gamma_{E,l}^{-1}u)^2 + (\gamma_{E,l}^{-2} - 1)D_{E,l}^2}{(1 - u^2 + 2i\gamma_{E,l}u + D_{E,l}^2 - \gamma_{E,l}^2 D_{E,l}^2)^{1/2}} \right]. \end{aligned} \quad (8)$$

Computations of the equilibrium Casimir-Polder force between nanoparticles and graphene-coated SiO₂ plate were performed by Eqs. (1), (3), (6), and (8). Since the force values quickly decrease with increasing separation, they were normalized either to the Casimir-Polder force F_0 between a nanoparticle and an ideal metal plane at zero temperature or to the classical limit F_{cl} reached in the same configuration, considered at temperature T_E at large separations [82,89]

$$F_0(a) = -\frac{3\hbar c}{2\pi a^5} \alpha(0), \quad F_{cl}(a, T_E) = -\frac{3k_B T_E}{4a^4} \alpha(0). \quad (9)$$

In Figure 1, the computational results for (a) $F_{eq}^{SiO_2}/F_0$ and (b) $F_{eq}^{SiO_2}/F_{cl}$ are presented as the function of separation for a graphene coating with the mass gap $\Delta = 0.2$ eV and chemical potential $\mu = 0, 0.075,$ and 0.15 eV (lines 1, 2, and 3, respectively). As is seen in Figure 1, the force magnitude increases with increasing chemical potential as it should be. At all separations considered the magnitude of $F_{eq}^{SiO_2}$ decreases with separation slower than $|F_0|$. At $a > 1 \mu\text{m}$, $|F_{eq}^{SiO_2}|$ decreases with separation faster than $|F_{cl}|$.

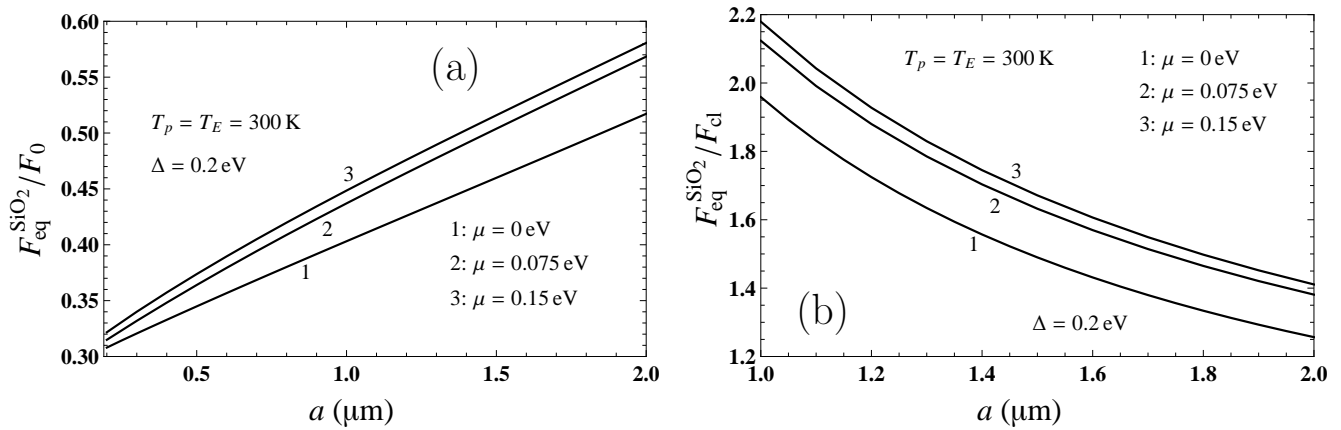


Figure 1. The equilibrium Casimir-Polder force between a nanoparticle and a graphene-coated SiO₂ plate at $T_p = T_E = 300$ K normalized to (a) the zero-temperature Casimir-Polder force from an ideal metal plane and (b) classical limit of the same force at $T_E = 300$ K is shown as the function of separation for a graphene coating with the mass gap $\Delta = 0.2$ eV and chemical potential $\mu = 0, 0.075,$ and 0.15 eV by the lines labeled 1, 2, and 3, respectively.

Next, let us consider the impact of the mass-gap parameter on the Casimir-Polder force. In Figure 2, the computational results for (a) $F_{eq}^{SiO_2}/F_0$ and (b) $F_{eq}^{SiO_2}/F_{cl}$ are presented as the function of separation by the pairs solid and dashed lines labeled 1 and 2. In pair 1, the mass-gap parameter $\Delta = 0.2$ eV for both lines, whereas the chemical potential $\mu = 0.075$ eV for the solid and 0 for the dashed line. In pair 2, the mass-gap parameter $\Delta = 0.1$ eV for both lines with the same values of μ , as in pair 1, for the solid and dashed lines.

As is seen in Figure 2, the force magnitude increases with decreasing value of the energy gap. This means that the chemical potential and the energy gap of graphene coating act on the Casimir-Polder force in the opposite directions. It is seen also that if $\mu \neq 0$ (see the solid lines) the dependence of the force value on Δ is much weaker than for graphene coating with $\mu = 0$ (see the dashed lines).

Note that numerical results presented in Figures 1 and 2 do not depend on $\alpha(0)$, i.e., on the nanoparticle radius. The absolute values of $F_{eq}^{SiO_2}$ can be obtained from Figures 1 and 2 by using Eq. (9) and the values of $\alpha(0)$ indicated above.

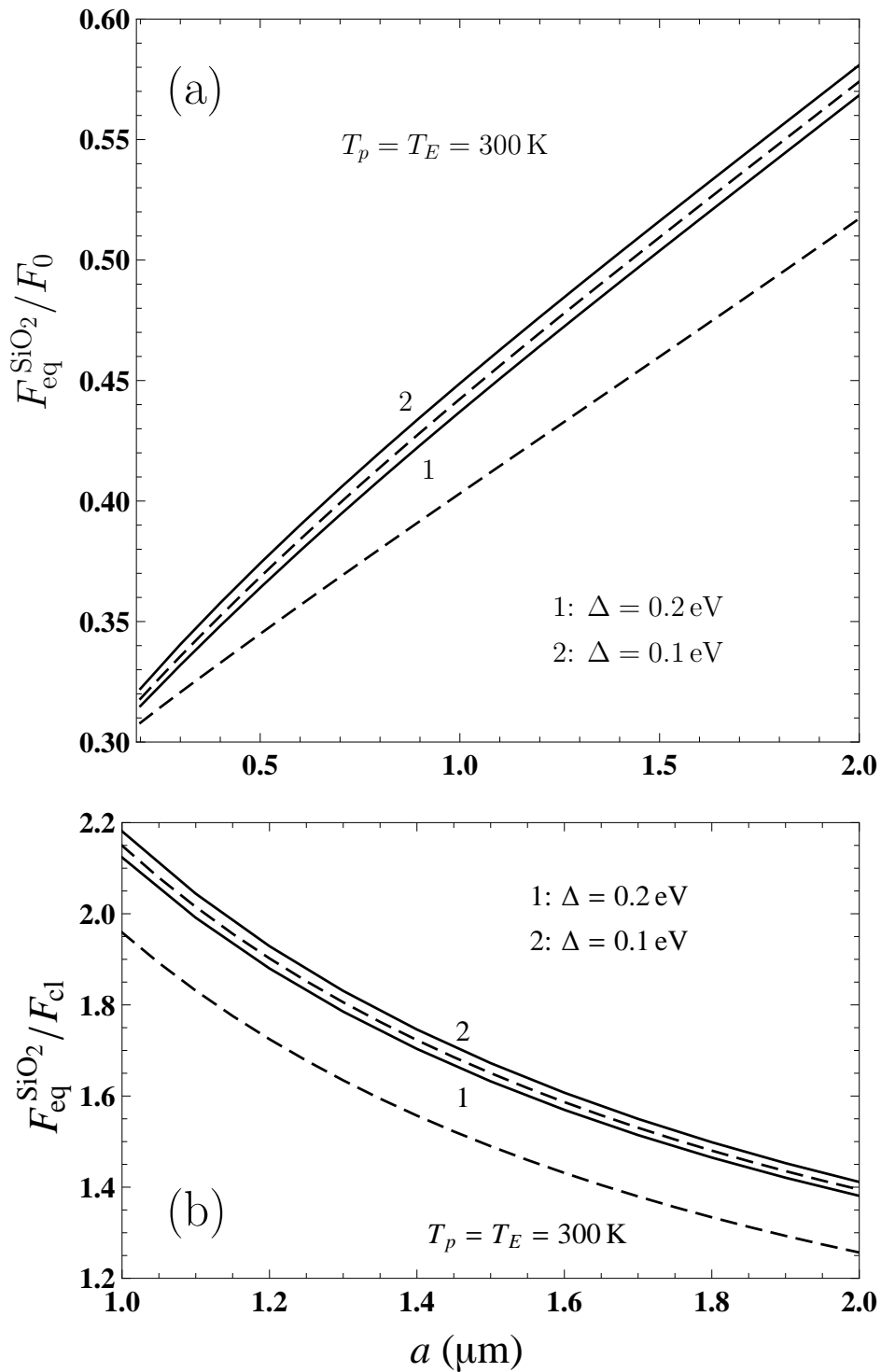


Figure 2. The equilibrium Casimir-Polder force between a nanoparticle and a graphene-coated SiO_2 plate at $T_p = T_E = 300 \text{ K}$ normalized to (a) the zero-temperature Casimir-Polder force from an ideal metal plane and (b) classical limit of the same force at $T_E = 300 \text{ K}$ is shown as the function of separation by the two pairs solid and dashed lines. In the pair labeled 1, the mass-gap parameter $\Delta = 0.2 \text{ eV}$ for both lines, whereas the chemical potential $\mu = 0.075 \text{ eV}$ for the solid line and 0 for the dashed line. In the pair labeled 2, $\Delta = 0.1 \text{ eV}$ for both lines with the same corresponding values of μ as in the pair 1.

3. Nonequilibrium Casimir-Polder Force between Nanoparticle and Plate Coated with Gapped and Doped Graphene: General Formalism

Now we consider the situation out of thermal equilibrium when the temperature of nanoparticles is equal to T_E , i.e., is the same as of the environment, whereas the temperature of the graphene-coated plate T_p can be either lower or higher than T_E .

In the generalization of the Lifshitz theory to out-of-thermal-equilibrium conditions, the nonequilibrium force is usually presented as the sum of two terms, one of which is akin the equilibrium force by its form and another one is a truly nonequilibrium term [55,57]. In the literature, different forms of these terms are contained leading to the same total result. Below, we represent the nonequilibrium Casimir-Polder force following Refs. [67,70,71]

$$F_{\text{neq}}^{\text{SiO}_2}(a, \Delta, \mu, T_E, T_p) = F_{\text{eq}}^{\text{SiO}_2}(a, \Delta, \mu, T_E, T_p) + F_r^{\text{SiO}_2}(a, \Delta, \mu, T_E, T_p). \quad (10)$$

Here, $F_{\text{eq}}^{\text{SiO}_2}$ was already defined in Eq. (1) as an equilibrium Casimir-Polder force, but now it has another meaning. In Eq. (1), it was assumed that $T_p = T_E = 300$ K, whereas now $T_p \neq T_E$ and, thus, $F_{\text{eq}}^{\text{SiO}_2}$, although resembles the equilibrium force by its form, describes some part of the effects of nonequilibrium.

The truly nonequilibrium contribution to Eq. (10) is given by [67,70,71]

$$F_r^{\text{SiO}_2}(a, \Delta, \mu, T_E, T_p) = \frac{2\hbar\alpha(0)}{\pi c^2} \int_0^\infty d\omega \Theta(\omega, T_E, T_p) \int_{\omega/c}^\infty k dk e^{-2aq(\omega, k)} \quad (11)$$

$$\times \text{Im} \left\{ \left[2q^2(\omega, k)c^2 + \omega^2 \right] R_{\text{TM}}(\omega, k, \Delta, \mu, T_p) + \omega^2 R_{\text{TE}}(\omega, k, \Delta, \mu, T_p) \right\},$$

where

$$\Theta(\omega, T_E, T_p) = \left(e^{\frac{\hbar\omega}{k_B T_E}} - 1 \right)^{-1} - \left(e^{\frac{\hbar\omega}{k_B T_p}} - 1 \right)^{-1}, \quad q(\omega, k) = \left(k^2 - \frac{\omega^2}{c^2} \right)^{1/2}. \quad (12)$$

The reflection coefficients in Eq. (11) are similar to those in Eq. (3), but now they are defined along the real frequency axis

$$R_{\text{TM}}(\omega, k, \Delta, \mu, T_p) = \frac{\hbar k^2 [\varepsilon(\omega)q(\omega, k) - q^\varepsilon(\omega, k)] + q(\omega, k)q^\varepsilon(\omega, k)\Pi_{00}(\omega, k, \Delta, \mu, T_p)}{\hbar k^2 [\varepsilon(\omega)q(\omega, k) + q^\varepsilon(\omega, k)] + q(\omega, k)q^\varepsilon(\omega, k)\Pi_{00}(\omega, k, \Delta, \mu, T_p)},$$

$$R_{\text{TE}}(\omega, k, \Delta, \mu, T_p) = \frac{\hbar k^2 [q(\omega, k) - q^\varepsilon(\omega, k)] - \Pi(\omega, k, \Delta, \mu, T_p)}{\hbar k^2 [q(\omega, k) + q^\varepsilon(\omega, k)] + \Pi(\omega, k, \Delta, \mu, T_p)} \quad (13)$$

where

$$q^\varepsilon(\omega, k) = \left[k^2 - \varepsilon(\omega) \frac{\omega^2}{c^2} \right]^{1/2},$$

$$\Pi(\omega, k, \Delta, \mu, T_p) = k^2 \Pi_\beta^\beta(\omega, k, \Delta, \mu, T_p) - q^2(\omega, k) \Pi_{00}(\omega, k, \Delta, \mu, T_p). \quad (14)$$

It is seen that Eq. (13) is obtained from Eq. (3) simply by putting $i\tilde{\zeta}_{E,l} = \omega$. However, the components of the polarization tensor (6) and (8) are rather complicated functions. They should be analytically continued from the imaginary to real frequency axis of the plane of complex frequency which is a nontrivial procedure.

The advantage of representation (10) is that the truly nonequilibrium contribution to it (11) contains an integration on only the evanescent waves. For these waves $k > \omega/c$ and the quantity $q(\omega, k)$ in the power of the exponent under the integral is real.

The analytic continuation of the polarization tensor to the real frequency axis under the condition $k > \omega/c$ is, nevertheless, rather involved. It takes different forms in the so-called plasmonic region [90]

$$\frac{\omega}{c} < k \leq \frac{\omega}{v_F} \approx 300 \frac{\omega}{c} \quad (15)$$

and in the region

$$300 \frac{\omega}{c} \approx \frac{\omega}{v_F} < k < \infty. \quad (16)$$

We begin with the plasmonic region (15). The analytic continuation of the polarization tensor to this region of the real frequency axis for a pristine and gapped graphene was performed in Refs. [67,70,71]. Here, we present the obtained results in a more convenient analytic form and generalize them for the case of gapped graphene with nonzero chemical potential.

As was shown in Ref. [48], the form of the sought for analytic continuation depends on whether $\hbar cp < \Delta$ or $\hbar cp \geq \Delta$ where $p \equiv p(\omega, k) = \sqrt{\omega^2 - v_F^2 k^2}/c$. If the inequality $\hbar cp(\omega, k) < \Delta$ is satisfied, the results of Ref. [48] for Π_{00} generalized for the case $\mu \neq 0$ can be identically represented in the following form:

$$\begin{aligned} \Pi_{00}(\omega, k, \Delta, \mu, T_p) &= -\frac{2\alpha k^2}{cp^2(\omega, k)} \Phi_1(\omega, k, \Delta) + \frac{4\alpha \hbar c^2 p(\omega, k)}{v_F^2} \int_{\tilde{D}}^{\infty} du \tilde{w}(u, \omega, k, \mu, T_p) \\ &\times \left[1 - \frac{1}{2cp(\omega, k)} \sum_{\lambda=\pm 1} \lambda B_1(cp(\omega, k)u + \lambda\omega) \right], \end{aligned} \quad (17)$$

where

$$\begin{aligned} \Phi_1(\omega, k, \Delta) &= \Delta - \hbar cp(\omega, k) \left[1 + \frac{\Delta^2}{\hbar^2 c^2 p^2(\omega, k)} \right] \operatorname{arctanh} \frac{\hbar cp(\omega, k)}{\Delta}, \\ \tilde{w}(u, \omega, k, \mu, T_p) &= \sum_{\kappa=\pm 1} \left[e^{\tilde{B}(\omega, k, T_p)u + \kappa \frac{\mu}{k_B T_p}} + 1 \right]^{-1}, \\ \tilde{D} \equiv \tilde{D}(\omega, k, \Delta) &= \frac{\Delta}{\hbar cp(\omega, k)}, \quad \tilde{B}(\omega, k, T_p) = \frac{\hbar cp(\omega, k)}{2k_B T_p}, \\ B_1(x) &= \frac{x^2 - v_F^2 k^2}{[x^2 - v_F^2 k^2 A(\omega, k, \Delta)]^{1/2}}, \quad A(\omega, k, \Delta) = 1 - \frac{\Delta^2}{\hbar^2 c^2 p^2(\omega, k)}. \end{aligned} \quad (18)$$

In the region $\hbar cp(\omega, k) < \Delta$ under consideration $A(\omega, k, \Delta) < 0$ and the quantity Π_{00} is real.

Using the same notations, for Π one obtains from Ref. [48]

$$\begin{aligned} \Pi(\omega, k, \Delta, \mu, T_p) &= \frac{2\alpha k^2}{c} \Phi_1(\omega, k, \Delta) + \frac{4\alpha \hbar \omega^2 p(\omega, k)}{v_F^2} \int_{\tilde{D}}^{\infty} du \tilde{w}(u, \omega, k, \mu, T_p) \\ &\times \left[1 - \frac{cp(\omega, k)}{2\omega^2} \sum_{\lambda=\pm 1} \lambda B_2(cp(\omega, k)u + \lambda\omega) \right], \end{aligned} \quad (19)$$

where

$$B_2(x) = \frac{x^2 + v_F^2 k^2 [1 - A(\omega, k, \Delta)]}{[x^2 - v_F^2 k^2 A(\omega, k, \Delta)]^{1/2}}. \quad (20)$$

The quantity Π is also the real function.

Now we consider the region of ω and k plane where the inequality $\hbar cp(\omega, k) \geq \Delta$ is satisfied. In this region, $A(\omega, k, \Delta) \geq 0$ and, as a consequence, the quantities Π_{00} and Π have both the real and imaginary parts. From the results of Ref. [48] generalized for the case $\mu \neq 0$, after identical transformations, one obtains

$$\begin{aligned} \Pi_{00}(\omega, k, \Delta, \mu, T_p) &= -\frac{2\alpha k^2}{cp^2(\omega, k)} \Phi_2(\omega, k, \Delta) + \frac{4\alpha \hbar c^2 p(\omega, k)}{v_F^2} \left\{ \int_{\tilde{D}}^{u_1} du \tilde{w}(u, \omega, k, \mu, T_p) \right. \\ &\times \left[1 - \frac{1}{2cp(\omega, k)} \sum_{\lambda=\pm 1} B_1(cp(\omega, k)u + \lambda\omega) \right] \\ &\left. + \int_{u_1}^{\infty} du \tilde{w}(u, \omega, k, \mu, T_p) \left[1 - \frac{1}{2cp(\omega, k)} \sum_{\lambda=\pm 1} \lambda B_1(cp(\omega, k)u + \lambda\omega) \right] \right\}, \end{aligned} \quad (21)$$

where

$$\Phi_2(\omega, k, \Delta) = \Delta - \hbar cp(\omega, k) \left[1 + \frac{\Delta^2}{\hbar^2 c^2 p^2(\omega, k)} \right] \left[\operatorname{arctanh} \frac{\Delta}{\hbar cp(\omega, k)} + i \frac{\pi}{2} \right] \quad (22)$$

and the roots of the common denominator of the functions B_1 and B_2 are

$$u_{1,2} = \frac{1}{cp(\omega, k)} \left[\omega \mp v_F k \sqrt{A(\omega, k, \Delta)} \right]. \quad (23)$$

These roots belonging to the integration domain $\tilde{D} < u_1 < u_2 < \infty$ are obtained for $\lambda = -1$.

In a similar manner, Π is given by

$$\begin{aligned} \Pi(\omega, k, \Delta, \mu, T_p) &= \frac{2\alpha k^2}{c} \Phi_2(\omega, k, \Delta) + \frac{4\alpha \hbar \omega^2 p(\omega, k)}{v_F^2} \left\{ \int_{\tilde{D}}^{u_1} du \tilde{w}(u, \omega, k, \mu, T_p) \right. \\ &\times \left[1 - \frac{cp(\omega, k)}{2\omega^2} \sum_{\lambda=\pm 1} B_2(cp(\omega, k)u + \lambda\omega) \right] \\ &\left. + \int_{u_1}^{\infty} du \tilde{w}(u, \omega, k, \mu, T_p) \left[1 - \frac{cp(\omega, k)}{2\omega^2} \sum_{\lambda=\pm 1} \lambda B_2(cp(\omega, k)u + \lambda\omega) \right] \right\}. \end{aligned} \quad (24)$$

Note that the imaginary parts of Π_{00} and Π arise in the second integrals in Eqs. (21) and (24) when integrating with respect to u from u_1 to u_2 .

Let us continue and consider the region (16). In this region, the analytic continuation of the polarization tensor (6) and (8) to the real frequency axis can be obtained by putting $i\zeta_{E,l} = \omega$ with the appropriate choice of the branch of the square root in denominator [48]. For this purpose, it is first convenient to represent the real part in Eqs. (6) and (8) as half a sum of the complex conjugated quantities. Then, the quantity Π_{00} in the region (16) of real frequency axis takes the form

$$\begin{aligned} \Pi_{00}(\omega, k, \Delta, \mu, T_p) &= \frac{\alpha \hbar k^2}{\tilde{q}(\omega, k)} \Psi(D) + \frac{4\alpha \hbar c^2 \tilde{q}(\omega, k)}{v_F^2} \int_D^{\infty} du w(u, \omega, k, \mu, T_p) \\ &\times \left\{ 1 - \frac{1}{2} \sum_{\lambda=\pm 1} \lambda \frac{1 - u^2 + 2\lambda \tilde{\gamma}(\omega, k)u}{[1 - u^2 + 2\lambda \tilde{\gamma}(\omega, k)u + D^2 + \tilde{\gamma}^2(\omega, k)D^2]^{1/2}} \right\}, \end{aligned} \quad (25)$$

where, in accordance with Eq. (7),

$$\begin{aligned}
\tilde{q}(\omega, k) &= \frac{1}{c} \sqrt{v_F^2 k^2 - \omega^2}, & \tilde{\gamma}(\omega, k) &= \frac{\omega}{\sqrt{v_F^2 k^2 - \omega^2}}, \\
D \equiv D(\omega, k, \Delta) &= \frac{\Delta}{\hbar c \tilde{q}(\omega, k)}, & B(\omega, k, T_p) &= \frac{\hbar c \tilde{q}(\omega, k)}{2k_B T_p} \\
w(u, \omega, k, \mu, T_p) &= \sum_{\kappa=\pm 1} \left[e^{B(\omega, k, T_p)u + \kappa \frac{\mu}{k_B T_p}} + 1 \right]^{-1}.
\end{aligned} \tag{26}$$

In a similar way, the analytic continuation of the quantity Π to the region (16) of real frequency axis is

$$\begin{aligned}
\Pi(\omega, k, \Delta, \mu, T_p) &= \alpha \hbar k^2 \tilde{q}(\omega, k) \Psi(D) + \frac{4\alpha \hbar \tilde{q}(\omega, k) \omega^2}{v_F^2} \int_D^\infty du w(u, \omega, k, \mu, T_p) \\
&\times \left\{ 1 - \frac{1}{2} \sum_{\lambda=\pm 1} \lambda \frac{[1 - \lambda \tilde{\gamma}^{-1}(\omega, k)u]^2 - [\tilde{\gamma}^{-2}(\omega, k) + 1]D^2}{[1 - u^2 + 2\lambda \tilde{\gamma}(\omega, k)u + D^2 + \tilde{\gamma}^2(\omega, k)D^2]^{1/2}} \right\}.
\end{aligned} \tag{27}$$

Let us discuss the obtained expressions for the polarization tensor of gapped and doped graphene along the real frequency axis. First of all let us note that the polarization tensor behaves differently depending on whether the inequality $\Delta > 2\mu$ or $\Delta \leq 2\mu$ is satisfied.

If $\Delta > 2\mu$ the powers of exponents in the definitions of \tilde{w} and w in Eqs. (18) and (26) are positive even at the lower integration limits $u = \tilde{D}$ and $u = D$ in Eqs. (17) and (19), (21) and (24), (25) and (27). This is true because from Eqs. (18) and (26) one obtains

$$\tilde{B}\tilde{D} = BD = \frac{\Delta}{2k_B T_p} > \frac{\mu}{k_B T_p}. \tag{28}$$

In this case, Eqs.(18) and (26) lead to

$$\lim_{T_p \rightarrow 0} w(u, \omega, k, \mu, T_p) = \lim_{T_p \rightarrow 0} \tilde{w}(u, \omega, k, \mu, T_p) = 0. \tag{29}$$

As a result, the polarization tensor at zero temperature defined as

$$\begin{aligned}
\Pi_{00}(\omega, k, \Delta, \mu, 0) &= \lim_{T_p \rightarrow 0} \Pi_{00}(\omega, k, \Delta, \mu, T_p), \\
\Pi(\omega, k, \Delta, \mu, 0) &= \lim_{T_p \rightarrow 0} \Pi(\omega, k, \Delta, \mu, T_p)
\end{aligned} \tag{30}$$

takes a much simplified form. It is equal to the first terms in Eqs. (17) and (19),

$$\begin{aligned}
\Pi_{00}(\omega, k, \Delta, \mu, 0) &= -\frac{2\alpha k^2}{cp^2(\omega, k)} \Phi_1(\omega, k, \Delta), \\
\Pi(\omega, k, \Delta, \mu, 0) &= \frac{2\alpha k^2}{c} \Phi_1(\omega, k, \Delta),
\end{aligned} \tag{31}$$

in the plasmonic region (15) under the condition $\hbar cp < \Delta$, to the first terms in Eqs. (21) and (24),

$$\begin{aligned}
\Pi_{00}(\omega, k, \Delta, \mu, 0) &= -\frac{2\alpha k^2}{cp^2(\omega, k)} \Phi_2(\omega, k, \Delta), \\
\Pi(\omega, k, \Delta, \mu, 0) &= \frac{2\alpha k^2}{c} \Phi_2(\omega, k, \Delta),
\end{aligned} \tag{32}$$

in the plasmonic region (15) under the condition $\hbar cp \geq \Delta$, and to the first terms in Eqs. (25) and (27),

$$\begin{aligned}\Pi_{00}(\omega, k, \Delta, \mu, 0) &= \frac{\alpha \hbar k^2}{\tilde{q}(\omega, k)} \Psi(D), \\ \Pi(\omega, k, \Delta, \mu, 0) &= \alpha \hbar k^2 \tilde{q}(\omega, k) \Psi(D),\end{aligned}\quad (33)$$

in the region (16).

Thus, if the inequality $\Delta > 2\mu$ is satisfied, the polarization tensor at zero temperature (30) does not depend on the chemical potential μ .

It is easily seen that under the opposite inequality $\Delta < 2\mu$ there are the intervals in the integration domains where the powers of exponents in the definitions of \tilde{w} and w in Eqs. (18) and (26) with $\kappa = -1$ are negative. Thus, in the plasmonic region (15) the power of exponent in \tilde{w} with $\kappa = -1$ is negative within the interval

$$\tilde{D} < u < u_0 = \frac{2\mu}{\hbar cp(\omega, k)}.\quad (34)$$

In a similar way, in the region (16) the power of exponent in w with $\kappa = -1$ is negative in the interval

$$D < u < \tilde{u}_0 = \frac{2\mu}{\hbar c\tilde{q}(\omega, k)}.\quad (35)$$

In both cases it holds

$$\lim_{T_p \rightarrow 0} w(u, \omega, k, \mu, T_p) = \lim_{T_p \rightarrow 0} \tilde{w}(u, \omega, k, \mu, T_p) = 1.\quad (36)$$

As a result, not only the first but all terms in Eqs. (17) and (19), (21) and (24), (25) and (27) contribute to the polarization tensor at zero temperature defined in Eq. (30).

By way of example, in the region (16) the polarization tensor of graphene with the mass gap and chemical potential satisfying the condition $\Delta < 2\mu$ takes the following form at $T = 0$:

$$\begin{aligned}\Pi_{00}(\omega, k, \Delta, \mu, 0) &= \frac{\alpha \hbar k^2}{\tilde{q}(\omega, k)} \Psi(D) + \frac{4\alpha \hbar c^2 \tilde{q}(\omega, k)}{v_F^2} \\ &\times \left\{ \frac{2\mu - \Delta}{\hbar c \tilde{q}(\omega, k)} - \frac{1}{2} \int_D^{\tilde{u}_0} du \sum_{\lambda=\pm 1} \lambda \frac{1 - u^2 + 2\lambda \tilde{\gamma}(\omega, k)u}{[1 - u^2 + 2\lambda \tilde{\gamma}(\omega, k)u + D^2 + \tilde{\gamma}^2(\omega, k)D^2]^{1/2}} \right\}, \\ \Pi(\omega, k, \Delta, \mu, 0) &= \alpha \hbar k^2 \tilde{q}(\omega, k) \Psi(D) + \frac{4\alpha \hbar \tilde{q}(\omega, k) \omega^2}{v_F^2} \\ &\times \left\{ \frac{2\mu - \Delta}{\hbar c \tilde{q}(\omega, k)} - \frac{1}{2} \int_D^{\tilde{u}_0} du \sum_{\lambda=\pm 1} \lambda \frac{[1 - \lambda \tilde{\gamma}^{-1}(\omega, k)u]^2 - [\tilde{\gamma}^{-2}(\omega, k) + 1]D^2}{[1 - u^2 + 2\lambda \tilde{\gamma}(\omega, k)u + D^2 + \tilde{\gamma}^2(\omega, k)D^2]^{1/2}} \right\},\end{aligned}\quad (37)$$

where the upper integration limit \tilde{u}_0 is defined in Eq. (35).

Thus, under the condition $\Delta < 2\mu$ the polarization tensor at zero temperature depends on the chemical potential μ through the terms in the figure brackets in Eq. (37) and similar terms surviving at $T = 0$ in Eqs. (17), (19) and (21), (24) valid in the plasmonic region.

Note that in the plasmonic region (15) the expression for the polarization tensor at zero temperature (32), found under the opposite condition $2\mu < \Delta \leq \hbar cp$ contains the pure imaginary part for some values of ω and k satisfying the inequality $\hbar cp \geq \Delta$. This is in line with the fact that additional contributions to the zero-temperature polarization tensor arising under the condition $\Delta < 2\mu$ also contain the imaginary parts. It is only a quantitative difference.

Another situation arises in the region (16) where $k > \omega/v_F$. Here, under the condition $\Delta > 2\mu$, the polarization tensor at zero temperature (33) is real, but under the condition $\Delta < 2\mu$ it gains some imaginary part depending on μ for some values of ω and k . This leads to important qualitative differences between the cases $\Delta > 2\mu$ and $\Delta < 2\mu$, which are demonstrated in Section 4 by the results of numerical computations.

4. Computational Results for the Nonequilibrium Casimir-Polder Force

In this section, the nonequilibrium Casimir-Polder force $F_{\text{neq}}^{\text{SiO}_2}$ from Eq. (10) between nanoparticles and a silica plate coated with a gapped and doped graphene sheet is computed using the formalism presented in Sections 2 and 3. As in Section 2, the temperatures of nanoparticles and of the environment are assumed to be equal to $T_E = 300$ K, whereas the temperature of the graphene-coated plate is either lower, $T_p = 77$ K, or higher, $T_p = 500$ K, than that of the environment. All computations were performed for typical values of the mass-gap parameter $\Delta = 0.1$ and 0.2 eV and the chemical potential $\mu = 0, 0.075$ and 0.15 eV of the graphene coating within the separation region from 200 nm to 2 μm .

Numerical computations of the first contribution $F_{\text{eq}}^{\text{SiO}_2}$ to $F_{\text{neq}}^{\text{SiO}_2}$ given by Eq. (1) were performed along the imaginary frequency axis as discussed in Section 2 but with $T_p \neq T_E$. The computational results for the second contribution $F_r^{\text{SiO}_2}$ to $F_{\text{neq}}^{\text{SiO}_2}$ were obtained by Eq. (11) using the polarization tensor of graphene along the real frequency axis defined for different values of ω and k in Eqs. (17) and (19), (21) and (24), (25) and (27). Numerical data for the real and imaginary parts of the dielectric permittivity of SiO_2 are taken from Ref. [85] (see also Ref. [71] for the graphical representation of these data). Note that numerical computations of $F_{\text{neq}}^{\text{SiO}_2}$ are much more complicated than those for $F_{\text{eq}}^{\text{SiO}_2}$ made along the imaginary frequency axis owing to the quick variation of the integrands. They were performed using the program utilizing the Gauss-Kronrod and double-exponential quadrature methods for numerical integration from the GNU scientific Library [91] and Boost C++ Libraries [92]. The program was written in the C++ programming language. It utilizes the OpenMP Library [93] for parallelism. The numerical computations were performed on a supercomputer of the Peter the Great Saint Petersburg Polytechnic University. Sufficiently high precision of the computational results was reached using the Boost Multiprecision Library [94].

We begin with the case when the SiO_2 plate coated with gapped and doped graphene is heated up to 500 K whereas the temperature of nanoparticles and of the environment here and below is always $T_E = 300$ K. The mass-gap parameter of graphene coating is $\Delta = 0.2$ eV, whereas the chemical potential can be equal to zero or take the values $\mu = 0.075$ eV and 0.15 eV. In Figure 3 the computational results for the nonequilibrium Casimir-Polder force normalized to (a) the zero-temperature Casimir-Polder force F_0 acting on a nanoparticle from an ideal metal plane and (b) the classical limit F_{cl} of the same force at $T_p = T_E = 300$ K [see Eq. (9)] are shown as the function of separation by the lines labeled 1, 2, and 3 for graphene coating with $\mu = 0, 0.075$, and 0.15 eV, respectively.

From Figure 3 it is seen that with increasing chemical potential the magnitude of the nonequilibrium Casimir-Polder force increases. Thus, in this respect the nonequilibrium force behaves in the same way as the equilibrium one. Note that the lines 1 and 2, for which $2\mu < \Delta = 0.2$ eV, are rather close to each other at all separations. The line 3, for which $2\mu > \Delta$, is further apart from the lines 1 and 2 at short separations but approach them at larger separations. Thus, for a heated graphene-coated plate there is no qualitative difference between the cases $2\mu < \Delta$ and $2\mu > \Delta$.

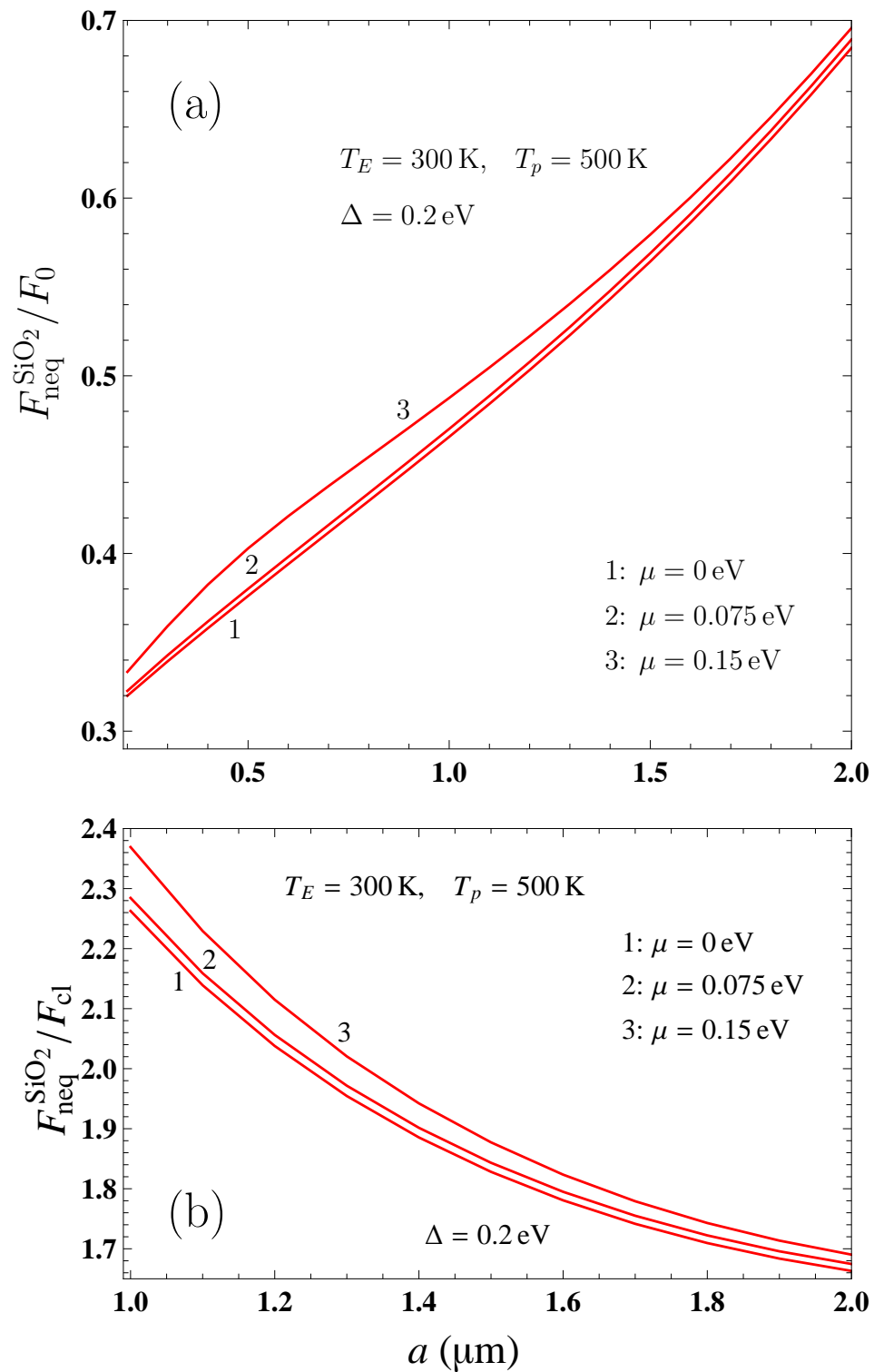


Figure 3. The nonequilibrium Casimir-Polder force between a nanoparticle and a graphene-coated SiO₂ plate kept at $T_p = 500$ K normalized to (a) the zero-temperature Casimir-Polder force from an ideal metal plane and (b) classical limit of the same force at $T_E = 300$ K is shown as the function of separation for a graphene coating with the mass gap $\Delta = 0.2$ eV and chemical potential $\mu = 0, 0.075$, and 0.15 eV by the lines labeled 1, 2, and 3, respectively.

Now we consider the situation when the graphene-coated plate is cooled to $T_p = 77$ K preserving unchanged all the other parameters of graphene coating listed in Figure 3.

The computational results for the normalized nonequilibrium Casimir-Polder force are presented as a function of separation in Figure 4 using the same notations for all lines as in Figure 3.

As is seen in Figure 4, the case of a cooled graphene-coated plate differ greatly from the case of a heated one. In the case of graphene-coated plate kept at $T_p = 77$ K, an impact of the chemical potential on the nonequilibrium Casimir-Polder force essentially depends on the relationship between 2μ and Δ .

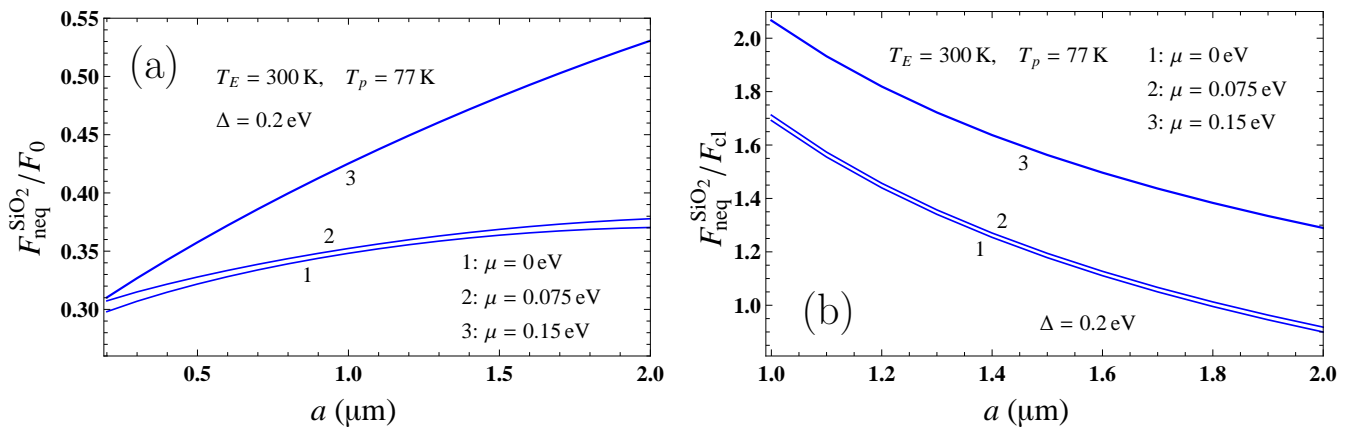


Figure 4. The nonequilibrium Casimir-Polder force between a nanoparticle and a graphene-coated SiO_2 plate at $T_p = 77$ K normalized to (a) the zero-temperature Casimir-Polder force from an ideal metal plane and (b) classical limit of the same force at $T_E = 300$ K is shown as the function of separation for a graphene coating with the mass gap $\Delta = 0.2$ eV and chemical potential $\mu = 0, 0.075$, and 0.15 eV by the lines labeled 1, 2, and 3, respectively.

If $2\mu < \Delta$ (this holds for the line labeled 2) the impact of nonzero μ on the force value is rather moderate. If, however, $2\mu > \Delta$ (line 3), this leads to significant deviation of the force value from that computed at $\mu = 0$ (line 1) which increases with increasing separation between nanoparticles and a graphene-coated plate. The enhancement of nonequilibrium force for the graphene coating with $2\mu > \Delta$ is explained by the increasing role of the polarization tensor at $T = 0$, which has a nonzero imaginary part in this case, and decrease of the thermal correction to it (see the discussion in the end of Section 3). By and large, although the nonequilibrium Casimir-Polder force increases with increasing μ for both the heated and cooled graphene-coated plate, in the latter case the impact of μ on the force value is much stronger.

We consider now the SiO_2 plate coated with the graphene sheet possessing the smaller mass-gap parameter $\Delta = 0.1$ eV and the moderate chemical potential $\mu = 0.075$ eV. In this case, the condition $2\mu > \Delta$ is satisfied. The nonequilibrium Casimir-Polder force acting on nanoparticles in such a configuration was computed at three different temperatures of the graphene-coated plate: $T_p = 77$ K (the cooled plate), $T_p = 300$ K (the situation of the thermal equilibrium), and $T_p = 500$ K (the heated plate).

The computational results for the Casimir-Polder force normalized to (a) the force F_0 from an ideal metal plane at zero temperature and (b) the classical force F_{cl} from an ideal metal plane at $T_p = T_E = 300$ K are shown in Figure 5 as the function of separation by the lines labeled 1, 2, and 3 for temperatures of the graphene-coated plate $T_p = 77$ K, 300 K, and 500 K, respectively. As is seen in Figure 5, the Casimir-Polder force at all separations increases with increasing temperature. This increase is smaller when the temperature of the graphene-coated plate T_p is below the temperature of the environment T_E and larger when $T_p > T_E$. In doing so, the impact of temperature on the force value increases with increasing separation.

It is interesting to consider the role of the mass-gap parameter. For this purpose, the same configuration at the same three temperatures of the graphene-coated plate was considered with the larger mass-gap parameter of the graphene sheet $\Delta = 0.2$ eV. In this case the opposite inequality $2\mu = 0.15$ eV $<$ Δ is satisfied.

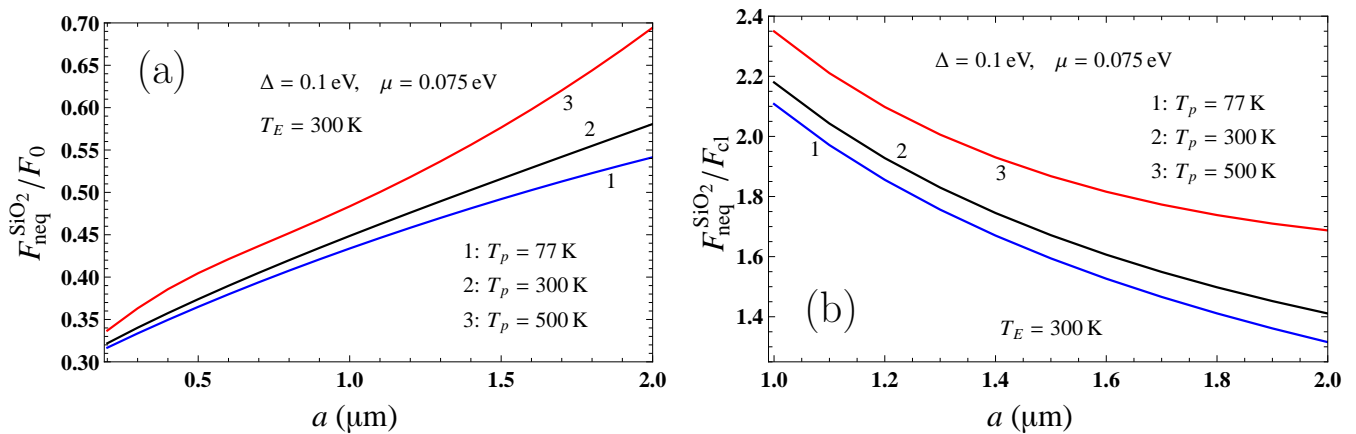


Figure 5. The Casimir-Polder force between a nanoparticle and a SiO₂ plate coated by a graphene sheet with the mass-gap parameter $\Delta = 0.1$ eV and chemical potential $\mu = 0.075$ eV normalized to (a) the Casimir-Polder force from an ideal metal plane at zero temperature and (b) classical limit of the same force at $T_E = 300$ K is shown as the function of separation for a graphene-coated plate temperatures $T_p = 77$ K (thermal nonequilibrium), $T_p = 300$ K (thermal equilibrium), and $T_p = 500$ K (thermal nonequilibrium) by the lines 1, 2, and 3, respectively.

The computational results for the nonequilibrium (lines 1 and 3) and equilibrium (line 2) Casimir-Polder force normalized to (a) F_0 and (b) F_{cl} are shown on Figure 6 by the lines labeled 1, 2, and 3 for temperatures of the graphene-coated plate $T_p = 77$ K, 300 K, and 500 K, respectively. Similar to Figure 5, the Casimir-Polder force increases with increasing temperature and this increase becomes larger at larger separations.

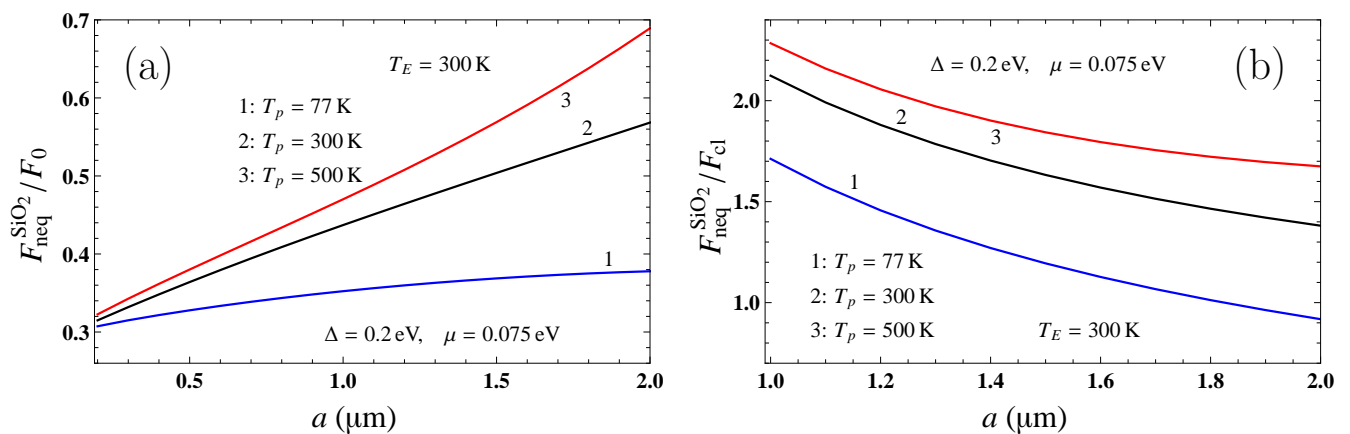


Figure 6. The Casimir-Polder force between a nanoparticle and a SiO₂ plate coated by a graphene sheet with the mass-gap parameter $\Delta = 0.2$ eV and chemical potential $\mu = 0.075$ eV normalized to (a) the Casimir-Polder force from an ideal metal plane at zero temperature and (b) classical limit of the same force at $T_E = 300$ K is shown as the function of separation for a graphene-coated plate temperatures $T_p = 77$ K (thermal nonequilibrium), $T_p = 300$ K (thermal equilibrium), and $T_p = 500$ K (thermal nonequilibrium) by the lines 1, 2, and 3, respectively.

By comparing the force values in Figure 5 and Figure 6, it is seen that at 77 K (the lines labeled 1 in both figures) the value of the nonequilibrium Casimir-Polder force for the graphene sheet with $\Delta = 0.1$ eV (Figure 5) is much larger than that for the graphene sheet with $\Delta = 0.2$ eV (Figure 6). This is because under the condition $2\mu > \Delta$ satisfied for the configuration considered in Figure 5 the impact of the polarization tensor at $T = 0$ is significantly increased as discussed in the end of Section 3. As to the force values shown by the lines 2 and 3, in Figure 6, where $2\mu < \Delta$, they are only slightly smaller than those in Figure 5.

Finally, we consider the same configuration, as in Figure 6, i.e., the SiO₂ plate coated by a graphene sheet with the mass-gap parameter $\Delta = 0.2$ eV, but with the twice as large chemical potential $\mu = 0.15$ eV. In this case, the condition $2\mu > \Delta$ is satisfied at the cost of sufficiently large μ , but not at the cost of relatively small Δ as in Figure 5. The computational results normalized to (a) F_0 and (b) F_{cl} are shown on Figure 7 as the function of separation by the lines 1 and 3 for the nonequilibrium Casimir-Polder force computed at $T_p = 77$ K and 500 K, respectively, and by the line 2 for the equilibrium force computed at $T_p = 300$ K.

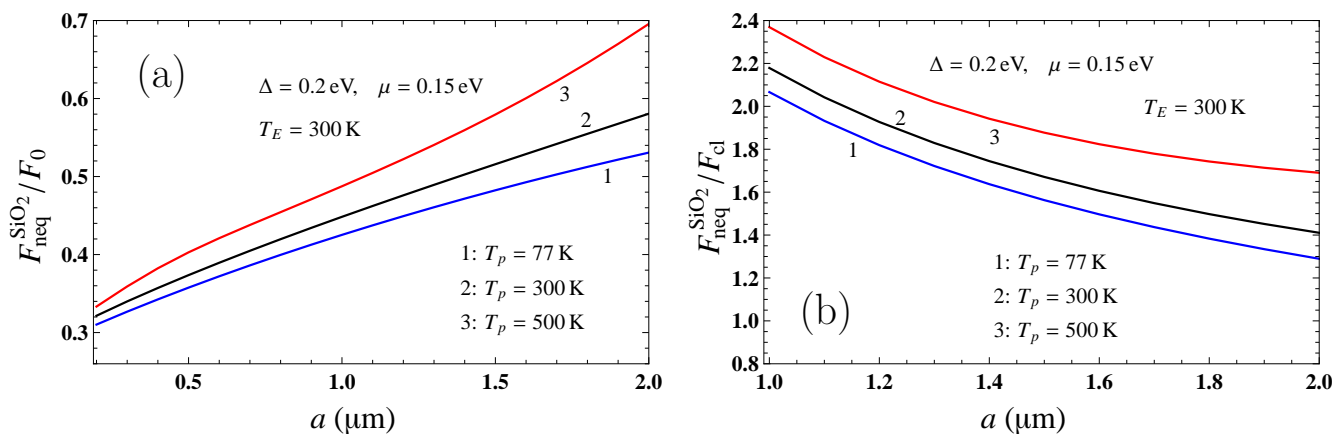


Figure 7. The Casimir-Polder force between a nanoparticle and a SiO₂ plate coated by a graphene sheet with the mass-gap parameter $\Delta = 0.2$ eV and chemical potential $\mu = 0.15$ eV normalized to (a) the Casimir-Polder force from an ideal metal plane at zero temperature and (b) classical limit of the same force at $T_E = 300$ K is shown as the function of separation for a graphene-coated plate temperatures $T_p = 77$ K (thermal nonequilibrium), $T_p = 300$ K (thermal equilibrium), and $T_p = 500$ K (thermal nonequilibrium) by the lines 1, 2, and 3, respectively.

Similar to the previous figures, the force values in Figure 7 increase with increasing temperature, and this increase is more pronounced at larger separations between nanoparticles and a graphene-coated plate. There is only a minor impact of the increased chemical potential on the lines 2 and 3 relevant to the equilibrium situation and to the heated graphene-coated plate, respectively. These lines demonstrate only slightly larger force values in comparison with those in Figure 6. One can conclude that at sufficiently high temperature the polarization tensor is almost independent on whether $2\mu > \Delta$ or $2\mu < \Delta$ although the zero-temperature contribution and the thermal correction to it are different under these conditions. As to the line 1 in Figure 7, computed at $T_p = 77$ K, it demonstrates much larger values of the nonequilibrium Casimir-Polder force than the line 1 in Figure 6. This effect is explained by the fact that at $2\mu > \Delta$ the polarization tensor at zero temperature takes the relatively large value. Specifically, it has a nonzero imaginary part in the region (16) (see a discussion in the end of Section 3). For a cooled plate just this region contributes to the increase of the force value.

5. Discussion

As was shown in Section 1, the Casimir-Polder interaction of nanoparticles with material substrates and, especially, with graphene-coated plates attracts much attention in fundamental physics and finds applications in nanotechnology. Because of this, it is important to reliably predict the strength of this interaction and its dependence on all relevant parameters. Graphene is a novel material and, to a first approximation, its response to the electromagnetic field was described by using different phenomenological approaches, such as Kubo theory, 2D Drude model etc. (see Refs. [2–4]) for a review).

Development of the formalism of the polarization tensor [46–49] has made it possible to calculate the equilibrium Casimir and Casimir-Polder forces in graphene systems in the framework of the Dirac model on the basis of first principles of thermal quantum field theory at nonzero temperature. However, application of the same formalism to the nonequilibrium forces, although rather straightforward theoretically, presents serious computational difficulties. The reason is that the equilibrium Casimir and Casimir-Polder forces are calculated as the sum over the discrete pure imaginary Matsubara frequencies, whereas computation of the nonequilibrium forces is unavoidably involved with the integration of rapidly varying functions along the real frequency axis [52–63], which was always challenging in the Casimir physics.

This difficulty was overcome step by step. At first, the nonequilibrium Casimir-Polder force between nanoparticles and a freestanding sheet of a pristine graphene was considered [67]. This case is interesting from the theoretical point of view, but does not reflect realistic experimental situations. Next, the impact of the mass gap, which exists in real graphene sheets, on the nonequilibrium force was investigated [70]. Among other things, the mass gap necessarily arises in graphene sheets deposited on some substrate. Because of this, the obtained results were generalized for the case of a graphene-coated dielectric plate [71] as usually takes place in experimental situations. All these computations demanded the use of a supercomputer.

One more important parameter, which was as yet disregarded, is the chemical potential reflecting the concentration of foreign atoms in a graphene sheet. As was shown previously, just the relationship between the mass gap and chemical potential determines the behavior of the Casimir and Casimir-Polder forces in graphene systems [40,42,44]. In Ref. [76] the impact of chemical potential on the nonequilibrium Casimir force between two parallel graphene-coated plates was investigated, but with disregarded mass gap of graphene and using the spatially local model of its electromagnetic response.

The formalism and computational results presented in this paper take into account all the parameters important for an adequate description of the nonequilibrium Casimir-Polder interaction between nanoparticles and a graphene-coated plate in the experimental situation, i.e., the mass gap and chemical potential of a graphene sheet, the dielectric permittivity of the plate material and their temperature. As expected from the experience obtained when studying the graphene systems in thermal equilibrium, the nonequilibrium Casimir-Polder force between nanoparticles and a graphene-coated substrate essentially depends on the relationship between the energy gap and twice the chemical potential of the graphene coating. This opens opportunities for high-reliability predictions of the Casimir-Polder forces in graphene systems out of thermal equilibrium for a subsequent comparison with the experimental data.

6. Conclusions

To conclude, in the foregoing we have investigated the Casimir-Polder force between spherical nanoparticles and a graphene-coated SiO₂ plate in out-of-thermal-equilibrium conditions. The response of graphene to the electromagnetic field was described by the spatially nonlocal polarization tensor taking into account both the mass gap and chemical potential of the graphene coating, which was found in the framework of the Dirac model. The plate material was characterized by the frequency-dependent dielectric permittivity obtained from the tabulated optical data for the complex index of refraction of silica glass.

By computing the nonequilibrium Casimir-Polder force on a supercomputer, the following results were obtained. With increasing chemical potential μ of the graphene coating, the nonequilibrium Casimir-Polder force increases for both heated and cooled graphene-coated plate. An impact of the chemical potential on the force value is stronger when the graphene-coated plate is cooled, as compared to the environment temperature, and weaker when it is heated. An impact of the mass gap Δ of the graphene coating is also more pronounced for a cooled graphene-coated plate. In this case, the character of the nonequilibrium Casimir-Polder force essentially depends on the relationship between the values of Δ and 2μ . An impact of the chemical potential on the force value is rather moderate if $2\mu < \Delta$, but if $2\mu > \Delta$ the magnitude of the nonequilibrium force becomes much larger than that computed for a graphene coating with $\mu = 0$. This effect is explained by the increasing role of the polarization tensor of graphene defined at zero temperature.

The magnitude of the nonequilibrium Casimir-Polder force increases with increasing temperature of the graphene-coated plate, all other conditions being equal. This increase is weaker and stronger if the temperature of the graphene-coated plate is lower and higher than that of the environment, respectively. In all cases the impact of temperature on the force value becomes stronger with increasing separation between nanoparticles and a graphene-coated plate.

To conclude, the revealed dependencies of the nonequilibrium Casimir-Polder force between nanoparticles and a graphene-coated plate from the mass-gap parameter, chemical potential, and temperature provide a way to control the force value in the graphene-based nanotechnological devices of next generations.

Funding: G.L.K. and V.M.M. were partially funded by the Ministry of Science and Higher Education of Russian Federation ("The World-Class Research Center: Advanced Digital Technologies," contract No. 075-15-2022-311 dated April 20, 2022). The research of V.M.M. was partially carried out in accordance with the Strategic Academic Leadership Program "Priority 2030" of the Kazan Federal University.

References

1. Geim, A.K.; Novoselov, K.S. The rise of graphene. *Nature Mater.* **2007**, *6*, 183–191.
2. Castro Neto, A.H.; Guinea, F.; Peres, N.M.R.; Novoselov, K.S.; Geim, A.K. The electronic properties of graphene. *Rev. Mod. Phys.* **2009**, *81*, 109–162.
3. Aoki, H.; Dresselhaus, M.S., (Eds.). *Physics of Graphene*; Springer: Cham, Switzerland, 2014.
4. Katsnelson, M.I. *The Physics of Graphene*; Cambridge University Press: Cambridge, UK, 2020.
5. Janavika, K.M.; Thangaraj, R.P. Graphene and its application: A review. *Materialstoday: Proc.*, <https://doi.org/10.1016/j.matpr.2023.05.446>.
6. Dehmiwal, S.; Bahuguna, M. Graphene – properties, production and rising applications: A review. *J. Mater. NanoSci.* **2021**, *8*, 51–63.
7. Williams, G.; Kamat, P.V. Graphene-Semiconductor Nanocomposites: Excited-State Interactions between ZnO Nanoparticles and Graphene Oxide. *Langmuir* **2009**, *25*, 13869–13873.
8. Das, B.; Choudhury, B.; Gomathi, A.; Manna, A.K.; Pati, S.K.; Rao, C.N.R. Interaction of Inorganic Nanoparticles with Graphene. *ChemPhysChem* **2011**, *12*, 937–943.
9. Biehs, S.-A.; Agarwal, G.S. Anisotropy enhancement of the Casimir-Polder force between a nanoparticle and graphene. *Phys. Rev. A* **2015**, *90*, 042510; Erratum in *Phys. Rev. A* **2015**, *91*, 039901.
10. Devi, J.M. Simulation Studies on the Interaction of Graphene and Gold Nanoparticle. *Int. J. Nanosci.* **2018**, *17*, 1760043.
11. Low, S.; Shon, Y.-S. Molecular interactions between pre-formed metal nanoparticles and graphene families. *Adv. Nano Res.* **2018**, *6*, 357–375.
12. Huang, L.-W.; Jeng, H.-T.; Su, W.-B.; Chang, C.-S. Indirect interactions of metal nanoparticles through graphene. *Carbon* **2021**, *174*, 132–137.
13. Casimir, H.B.G.; Polder, D. The influence of retardation on the London-van der Waals forces. *Phys. Rev.* **1948**, *73*, 360–372.
14. Derjaguin, V.B.; Dzyaloshinsky, I.E.; Koptelova, M.M.; Pitaevsky, L.P. Molecular-Surface Forces in Binary Solutions. *Discuss. Faraday Soc.* **1965**, *40*, 246–252.
15. Parsegian, V.A. Formulae for the electrodynamic interaction of point particles with a substrate. *Mol. Phys.* **1974**, *27*, 1503–1511.
16. Lifshitz, E.M.; Pitaevskii, L.P. *Statistical Physics, Part II*; Pergamon: Oxford, UK, 1980.
17. Leanhardt, A.E.; Shin, Y.; Chikkatur, A.P.; Kielpinski, D.; Ketterle, W.; Pritchard, D.E. Bose-Einstein Condensates near a Microfabricated Surface. *Phys. Rev. Lett.* **2003**, *90*, 100404.

18. Babb, J.F.; Klimchitskaya, G.L.; Mostepanenko, V.M. Casimir-Polder interaction between an atom and a cavity wall under the influence of real conditions. *Phys. Rev. A* **2004**, *70*, 042901.
19. Caride, A.O.; Klimchitskaya, G.L.; Mostepanenko, V.M.; Zanette, S.I. Dependences of the van der Waals atom-wall interaction on atomic and material properties. *Phys. Rev. A* **2005**, *71*, 042901.
20. Babb, J.F. Long-range atom-surface interactions for cold atoms. *J. Phys.: Conf. Ser.* **2005**, *19*, 1–9.
21. Safari, H.; Welsch, D.-G.; Buhmann, S.Y.; Scheel, S. van der Waals potentials of paramagnetic atoms. *Phys. Rev. A* **2008**, *78*, 062901.
22. Bimonte, G.; Klimchitskaya, G.L.; Mostepanenko, V.M. Impact of magnetic properties on atom-wall interactions. *Phys. Rev. A* **2009**, *79*, 042906.
23. Haakh, H.; Intravaia, F.; Henkel, C.; Spagnolo, S.; Passante, R.; Power, B.; Sols, F. Temperature dependence of the magnetic Casimir-Polder interaction. *Phys. Rev. A* **2009**, *80*, 062905.
24. Ellingsen, S.Å.; Buhmann, S.Y.; Scheel, S. Temperature-Independent Casimir-Polder Forces Despite Large Thermal Photon Numbers. *Phys. Rev. Lett.* **2010**, *104*, 223003.
25. Judd, T.E.; Scott, R.G.; Martin, A.M.; Kaczmarek, B.; Fromhold, T.M. Quantum reflection of ultracold atoms from thin films, graphene and semiconductor heterostructures. *New J. Phys.* **2011**, *13*, 083020.
26. Passante, R.; Rizzuto, L.; Spagnolo, S.; Tanaka, S.; Petrosky, T.Y. Harmonic oscillator model for the atom-surface Casimir-Polder interaction energy. *Phys. Rev. A* **2012**, *85*, 062109.
27. Chaichian, M.; Klimchitskaya, G.L.; Mostepanenko, V.M.; Tureanu, A. Thermal Casimir-Polder interaction of different atoms with graphene. *Phys. Rev. A* **2012**, *86*, 012515.
28. Arora, B.; Kaur, H.; Sahoo, B.K. C_3 coefficients for the alkali atoms interacting with a graphene and carbon nanotube. *J. Phys. B* **2014**, *47*, 155002.
29. Sun, W. Interaction forces between a spherical nanoparticle and a flat surface. *Phys. Chem. Chem. Phys.* **2014**, *16*, 5846–5854.
30. Kaur, K.; Kaur, J.; Arora, B.; Sahoo, B.K. Emending thermal dispersion interaction of Li, Na, K and Rb alkali-metal atoms with graphene in the Dirac model. *Phys. Rev. B* **2014**, *90*, 245405.
31. Klimchitskaya, G.L.; Mostepanenko, V.M. Impact of graphene coating on the atom-plate interaction. *Phys. Rev. A* **2014**, *89*, 062508.
32. Cysne, T.; Kort-Kamp, W.J.M.; Oliver, D.; Pinheiro, F.A.; Rosa, F.S.S.; Farina, C. Tuning the Casimir-Polder interaction via magneto-optical effects in graphene. *Phys. Rev. A* **2014**, *90*, 052511.
33. Kaur, K.; Arora, B.; Sahoo, B.K. Dispersion coefficients for the interactions of the alkali-metal and alkaline-earth-metal ions and inert-gas atoms with a graphene layer. *Phys. Rev. A* **2015**, *92*, 032704.
34. Bimonte, G.; Emig, T.; Kardar, M. Casimir-Polder force between anisotropic nanoparticles and gently curved surfaces. *Phys. Rev. D* **2015**, *92*, 025028.
35. Khusnutdinov, N.; Kashapov, R.; Woods, L.M. Casimir-Polder effect for a stack of conductive planes. *Phys. Rev. A* **2016**, *94*, 012513.
36. Fuchs, S.; Crosse, J.A.; Buhmann, S.Y. Casimir-Polder shift and decay rate in the presence of nonreciprocal media. *Phys. Rev. A* **2017**, *95*, 023805.
37. Rojas-Lorenzo, G.; Rubayo-Soneira, J.; Miret-Artés, S.; Pollak, E. Quantum reflection of rare-gas atoms and clusters from a grating. *Phys. Rev. A* **2018**, *98*, 063604.
38. Fuchs, S.; Bennett, R.; Krems, R.V.; Buhmann, S.Y. Nonadditivity of Optical and Casimir-Polder Potentials. *Phys. Rev. Lett.* **2018**, *121*, 083603.
39. Bordag, M.; Klimchitskaya, G.L.; Mostepanenko, V.M. Nonperturbative theory of atom-surface interaction: corrections at short separations. *J. Phys.: Condens. Matter* **2018**, *30*, 055003.
40. Henkel, C.; Klimchitskaya, G.L.; Mostepanenko, V.M. Influence of the chemical potential on the Casimir-Polder interaction between an atom and gapped graphene or a graphene-coated substrate. *Phys. Rev. A* **2018**, *97*, 032504.
41. Khusnutdinov, N.; Kashapov, R.; Woods, L.M. Thermal Casimir and Casimir-Polder interactions in N parallel 2D Dirac materials. *2D Mater.* **2018**, *5*, 035032.
42. Klimchitskaya, G.L.; Mostepanenko, V.M. Nernst heat theorem for an atom interacting with graphene: Dirac model with nonzero energy gap and chemical potential. *Phys. Rev. D* **2020**, *101*, 116003.
43. Khusnutdinov, N.; Emelianova, N. The Low-Temperature Expansion of the Casimir-Polder Free Energy of an Atom with Graphene. *Universe* **2021**, *7*, 70.
44. Klimchitskaya, G.L.; Mostepanenko, V.M. Casimir and Casimir-Polder Forces in Graphene Systems: Quantum Field Theoretical Description and Thermodynamics. *Universe* **2020**, *6*, 150.
45. Klimchitskaya, G.L.; Mostepanenko, V.M. The Casimir Force between Two Graphene Sheets: 2D Fresnel Reflection Coefficients, Contributions of Different Polarizations, and the Role of Evanescent Waves. *Physics* **2023**, *5*, 1013–1030.
46. Bordag, M.; Fialkovsky, I.V.; Gitman, D.M.; Vassilevich, D.V. Casimir interaction between a perfect conductor and graphene described by the Dirac model. *Phys. Rev. B* **2009**, *80*, 245406.
47. Fialkovsky, I.V.; Marachevsky, V.N.; Vassilevich, D.V. Finite-temperature Casimir effect for graphene. *Phys. Rev. B* **2011**, *84*, 035446.
48. Bordag, M.; Klimchitskaya, G.L.; Mostepanenko, V.M.; Petrov, V.M. Quantum field theoretical description for the reflectivity of graphene. *Phys. Rev. D* **2015**, *91*, 045037; Erratum in *Phys. Rev. D* **2016**, *93*, 089907.
49. Bordag, M.; Fialkovskiy, I.; Vassilevich, D. Enhanced Casimir effect for doped graphene. *Phys. Rev. B* **2016**, *93*, 075414; Erratum in *Phys. Rev. B* **2017**, *95*, 119905.

50. Yan, H.; Wang, J.; Feng, B.; Duan, K.; Weng, J. Graphene and Ag nanowires co-modified photoanodes for high-efficiency dye-sensitized solar cells. *Solar Energy* **2015**, *122*, 966–975.
51. Huang, K.; Yan, Y.; Yu, X.; Zhang, H.; Yang, D. Graphene coupled with Pt cubic nanoparticles for high performance, air-stable graphene-silicon solar cells. *Nano Energy* **2017**, *32*, 225–231.
52. Dorofeyev, I.A. The force of attraction between two solids with different temperatures. *J. Phys. A Math. Gen.* **1998**, *31*, 4369–4380.
53. Henkel, C.; Joulain, K.; Mulet, J.P.; Greffet, J.J. Radiation forces on small particles in thermal near fields. *J. Opt. A Pure Appl. Opt.* **2002**, *4*, S109–114.
54. Antezza, M.; Pitaevskii, L.P.; Stringari, S. New Asymptotic Behavior of the Surface-Atom Force out of Thermal Equilibrium. *Phys. Rev. Lett.* **2005**, *95*, 113202.
55. Antezza, M.; Pitaevskii, L.P.; Stringari, S.; Svetovoy, V.B. Casimir-Lifshitz force out of thermal equilibrium. *Phys. Rev. A* **2008**, *77*, 022901.
56. Bimonte, G. Scattering approach to Casimir forces and radiative heat transfer for nanostructured surfaces out of thermal equilibrium. *Phys. Rev. A* **2009**, *80*, 042102.
57. Messina, R.; Antezza, M. Scattering-matrix approach to Casimir-Lifshitz force and heat transfer out of thermal equilibrium between arbitrary bodies. *Phys. Rev. A* **2011**, *84*, 042102.
58. Bimonte, G.; Emig, T.; Krüger, M.; Kardar, M. Dilution and resonance-enhanced repulsion in nonequilibrium fluctuation forces. *Phys. Rev. A* **2011**, *84*, 042503.
59. Krüger, M.; Emig, T.; Bimonte, G.; Kardar, M. Non-equilibrium Casimir forces: Spheres and sphere-plate. *Europhys. Lett.* **2011**, *95*, 21002.
60. Krüger, M.; Bimonte, G.; Emig, T.; Kardar, M. Trace formulas for nonequilibrium Casimir interactions, heat radiation, and heat transfer for arbitrary bodies. *Phys. Rev. B* **2012**, *86*, 115423.
61. Klimchitskaya, G.L.; Mostepanenko, V.M.; Sedmik, R.I.P. Casimir pressure between metallic plates out of thermal equilibrium: Proposed test for the relaxation properties of free electrons. *Phys. Rev. A* **2019**, *100*, 022511.
62. Klimchitskaya, G.L.; Mostepanenko, V.M. Casimir-Polder Interaction of an Atom with a Cavity Wall Made of Phase-Change Material out of Thermal Equilibrium. *Atoms* **2020**, *9*, 4.
63. Ingold, G.-L.; Klimchitskaya, G.L.; Mostepanenko, V.M. Nonequilibrium effects in the Casimir force between two similar metallic plates kept at different temperatures. *Phys. Rev. A* **2020**, *101*, 032506.
64. Khandekar, C.; Buddhiraju, S.; Wilkinson, P.R.; Gimzewski, J.K.; Rodriguez, A.W.; Chase, C.; Fan, S. Nonequilibrium lateral force and torque by thermally excited nonreciprocal surface electromagnetic waves. *Phys. Rev. B* **2021**, *104*, 245433.
65. Castillo-López, S.G.; Esquivel-Sirvent, R.; Pirruccio, G.; Villarreal, C. Casimir forces out of thermal equilibrium near a superconducting transition. *Sci. Rep.* **2022**, *12*, 2905.
66. Obrecht, J.M.; Wild, R.J.; Antezza, M.; Pitaevskii, L.P.; Stringari, S.; Cornell, E.A. Measurement of the temperature dependence of the Casimir-Polder force. *Phys. Rev. Lett.* **2007**, *98*, 063201.
67. Klimchitskaya, G.L.; Mostepanenko, V.M.; Tsybin, O.Yu. Casimir-Polder attraction and repulsion between nanoparticles and graphene in out-of-thermal-equilibrium conditions. *Phys. Rev. B* **2022**, *105*, 195430; Erratum. *Phys. Rev. B* **2024**, *109*, 079901.
68. Gusynin, V.P.; Sharapov, S.G.; Carbotte, J.P. On the universal ac optical background in graphene. *New J. Phys.* **2009**, *11*, 095013.
69. Pyatkovsky, P.K. Dynamical polarization, screening, and plasmons in gapped graphene. *J. Phys. Condens. Matter* **2009**, *21*, 025506.
70. Klimchitskaya, G.L.; Korikov, C.C.; Mostepanenko, V.M.; Tsybin, O.Yu. Impact of Mass-Gap on the Dispersion Interaction of Nanoparticles with Graphene out of Thermal Equilibrium. *Appl. Sci.* **2023**, *13*, 7511.
71. Klimchitskaya, G.L.; Korikov, C.C.; Mostepanenko, V.M.; Tsybin, O.Yu. Nonequilibrium Casimir-Polder Interaction Between Nanoparticles and Substrates Coated with Gapped Graphene. *Symmetry* **2023**, *15*, 1580; Correction. *Symmetry* **2024**, *16*, 274.
72. Falkovsky, L.A. Optical properties of graphene. *J. Phys.: Conf. Series* **2008**, *129*, 012004.
73. Falkovsky, L.A. Thermodynamics of electron-hole liquids in graphene. *Pis'ma v ZhETF* **2013**, *98*, 183–186; Translated *JETP Lett.* **2013**, *98*, 161–164.
74. Liu, M.; Zhang, Y.; Klimchitskaya, G.L.; Mostepanenko, V.M.; Mohideen, U. Demonstration of Unusual Thermal Effect in the Casimir Force from Graphene. *Phys. Rev. Lett.* **2021**, *126*, 206802.
75. Liu, M.; Zhang, Y.; Klimchitskaya, G.L.; Mostepanenko, V.M.; Mohideen, U. Experimental and theoretical investigation of the thermal effect in the Casimir interaction from graphene. *Phys. Rev. B* **2021**, *104*, 085436.
76. Jeyar, Y.; Austry, K.; Luo, M.; Guizal, B.; Chan, H.B.; Antezza, M. Casimir-Lifshitz force between graphene-based structures out of thermal equilibrium. *Phys. Rev. B* **2023**, *108*, 115412.
77. Falkovsky, L.A.; Varlamov, A.A. Space-time dispersion of graphene conductivity. *Eur. Phys. J. B* **2007**, *56*, 281–284.
78. Hong, S.-Y.; Dadap, J.I.; Petrone, N.; Yeh, P.-C.; Hone, J.; Osgood, Jr., R.M. Optical Third-Harmonic Generation in Graphene. *Phys. Rev. X* **2013**, *3*, 021014.
79. Li, H.; He, P.; Yu, J.; Lee, L.J.; Yi, A.Y. Localized rapid heating process for precision chalcogenide glass molding. *Opt. Lasers Engineer.* **2015**, *73*, 62–68.
80. Marchena, M.; Song, Z.; Senaratne, W.; Li, C.; Liu, X.; Baker, D.; Ferrer, J.C.; Mazumder, P.; Soni, K.; Lee, R.; Pruneri, V. Direct growth of 2D and 3D graphene nano-structures over large glass substrates by tuning a sacrificial Cu-template layer. *2D Mater.* **2017**, *4*, 025088.

81. Yuan, Y.; Wang, Y.; Liu, S.; Zhang, X.; Liu, X.; Sun, C.; Yuan, D.; Zhang, Y.; Cao, X. Direct chemical vapor deposition synthesis of graphene super-hydrophobic transparent glass. *Vacuum* **2022**, *202*, 111136.
82. Bordag, M.; Klimchitskaya, G.L.; Mohideen, U.; Mostepanenko, V.M. *Advances in the Casimir Effect*; Oxford University Press: Oxford, UK, 2015.
83. Sernelius, B.E. *Fundamentals of van der Waals and Casimir Interactions*; Springer: New York, NY, USA, 2018.
84. Klimchitskaya, G.L.; Mohideen, U.; Mostepanenko, V.M. Theory of the Casimir interaction from graphene-coated substrates using the polarization tensor and comparison with experiment. *Phys. Rev. B* **2014**, *89*, 115419.
85. Palik, E.D., (Ed.). *Handbook of Optical Constants of Solids*; Academic Press: New York, NY, USA, 1985.
86. Hough, D.B.; White, L.R. The calculation of Hamaker constants from Lifshitz theory with applications to wetting phenomena. *Adv. Coll. Interface Sci.* **1980**, *14*, 3–41.
87. Bergström L. Hamaker constants in inorganic materials. *Adv. Coll. Interface Sci.* **1997**, *70*, 125–169.
88. Zhu, T.; Antezza, M.; Wang, J.-S. Dynamical polarizability of graphene with spatial dispersion. *Phys. Rev. B* **2021**, *103*, 125421.
89. Klimchitskaya, G.L.; Mohideen, U.; Mostepanenko, V.M. The Casimir force between real materials: Experiment and theory. *Rev. Mod. Phys.* **2009**, *81*, 1827–1885.
90. Bordag, M.; Pirozhenko, I.G. Surface plasmon on graphene at finite T . *Int. J. Mod. Phys. B* **2016**, *30*, 1650120.
91. Galassi, M.; Davies, J.; Theiler, J.; Gough, B.; Gungman, G.; Alken, P.; Booth, M.; Rossi, F.; Ulerich, R. GNU Scientific Library Reference Manual, 2021. Available online: <https://www.gnu.org/software/gsl/doc/latex/gsl-ref.pdf> (accessed on 1 December 2023).
92. Boost C++ Libraries. Available online: <https://www.boost.org> (accessed on 1 December 2023).
93. OpenMP Application Programming Interface. Available online: <https://www.openmp.org/specifications> (accessed on 1 December 2023).
94. Boost Multiprecision Library. Available online: <https://github.com/boostorg/multiprecision> (accessed on 1 December 2023).